Appl Nanosci (2016) 6:1149–1157
DOI 10.1007/s13204-016-0526-y

ORIGINAL ARTICLE

Lithium storage study on MoO_3-grafted TiO_2 nanotube arrays

Tauseef Anwar[1] · Li Wang[1] · Li Jiaoyang[1] · Wang Chen[2] · Rizwan Ur Rehman Sagar[3] · Liang Tongxiang[2]

Received: 8 January 2016 / Accepted: 27 February 2016 / Published online: 16 March 2016

Abstract Titanium dioxide nanotube arrays (TNAs) were fabricated via anodic ionization. Porous MoO_3 was grafted on TNAs with the help of hydrothermal method. Scanning electron microscopy and X-ray powder diffraction was utilized for the confirmation of one dimensional morphology and phase identification. The porous MoO_3 nanoflake-grafted TNAs (MoO_3/TNAs) electrode was used as anode material in lithium ion battery (LIB) and it was found that the areal specific capacity of MoO_3/TNAs ($\sim$797 μAh cm^{-2}) was three times higher than those of anatase TNAs ($\sim$287 μAh cm^{-2}) and porous MoO_3 ($\sim$234 μAh cm^{-2}) at 50 μA cm^{-2}.

Keywords Molybdenum oxide · Titanium dioxide nanotube arrays (TNAs) · Anode · Lithium-ion batteries (LIBs)

Introduction

Lithium ion battery (LIB) is one of the most reliable power sources for portable electronic devices. The improved performance of microbatteries is highly necessary for modern microelectronic devices such as PC memory, microelectromechanical systems (MEMS), medical implants, hearing aids, "smart" cards, RF-ID tags, remote sensors and energy harvesters, etc. (Kyerematen 2014; Matiko et al. 2014; Patil et al. 2008; Pikul et al. 2013). The requirement of high-performance LIBs encourages scientists to develop new anode materials with capacity higher than graphite (Reddy et al. 2013; Wu et al. 2012a; Wu and Hong 2014; Xiong et al. 2014). TiO_2 is a promising material for lithium storage due to its low volume expansion, environmental benignity and widespread availability. Amongst the various nanostructures of TiO_2 (Armstrong et al. 2006; Cao et al. 2010; Liu et al. 2012; Qiu et al. 2010; Ren et al. 2012; Wang et al. 2011), titanium dioxide nanotube arrays (TNAs) (Guo et al. 2012) are favorable due to their high specific surface area, high porosity, vertical orientation which accommodate volume expansion and also provide short lithium ion diffusion path (Wu et al. 2012b). However, the areal specific capacity, even for the optimized TNAs, is found to be low (Tauseef Anwar et al. 2015). Three different methods have been proposed to enhance the specific capacity: (1) doping TNAs with metal or nonmetal elements (Kyerematen et al. 2013b; Liu et al. 2008, 2009); (2) coating TNAs with conductive reagents (Guan and Wang 2013; Kim et al. 2010; Zhang et al. 2009); (3) modify TNAs with oxide materials that have larger capacities [SnO_2 (Meng et al. 2013), Co_3O_4 (Fan et al. 2013; Kyerematen et al. 2013a), Nb_2O_5 (Yang et al. 2013) and Fe_2O_3 (Yu et al. 2013)] to yield hybrid or composite structures.

Electronic supplementary material The online version of this article (doi:10.1007/s13204-016-0526-y) contains supplementary material, which is available to authorized users.

✉ Liang Tongxiang
txliang@tsinghua.edu.cn

[1] Beijing Key Lab of Fine Ceramics, Institute of Nuclear and New Energy Technology, Tsinghua University, Beijing 100084, People's Republic of China

[2] State Key Lab of New Ceramic and Fine Processing, Tsinghua University, Beijing 100084, People's Republic of China

[3] Nanshan District Key Lab for Biopolymers and Safety Evaluation, College of Materials Science and Engineering, Shenzhen University, Shenzhen 518060, People's Republic of China

MoO_3 is an anode material candidate due to its high theoretical capacity (1117 mAh g^{-1}). The orthorhombic phase layered structure of α-MoO_3 hosts Li^+ by insertion and deinsertion reaction. However, the electrochemical properties of TNAs could be further enhanced with the extra porous hybrid material such as MoO_3 (Fan et al. 2013; Guan et al. 2014a, b; Kyerematen et al. 2013a; Meng et al. 2013; Wang et al. 2013; Xue et al. 2011; Zhu et al. 2015). Considering low electronic conductivity and high volume expansion, Yu et al. (2014) synthesized porous MoO_3 thin films and elucidated better performance as compared to bulk MoO_3. Zhao et al. (2013) synthesized porous MoO_3 thin films via electro-deposition which exhibit a high capacity of 650 mAh g^{-1} at high current density of 3 A g^{-1}. Yu et al. synthesized porous MoO_3 nanosheets by hydrothermal method at Ti substrate and the nanosheets showed specific capacity of 750 mAh g^{-1} at 1C-rate. There are rare reports on the MoO_3/TNAs as anode material in LIBs. However, different fabrication of coating MoO_3 on TNAs led difference in their electrochemical properties. The hydrothermal synthesis for the grafting of MoO_3 nanoflakes at TNAs was used first time. The fabrication method and porosity would play important role for future electrochemical properties of material.

Herein, TNAs were grown at Ti substrate and consecutive annealing transforms TNAs in anatase phase. The porous MoO_3 were grafted using a facile hydrothermal method which facilitate high yield product (Fig. 1) (Fan et al. 2015a, b; Gong et al. 2015). The grafting of porous MoO_3 nanoflakes at TNAs was controlled via hydrothermal reaction time. The electrochemical properties were optimized by controlling thickness of MoO_3 with hydrothermal duration. There are several benefits of utilizing MoO_3/TNAs as electrode in LIBs. Firstly, TiO_2 with zero strain (ca. 4 % volume change after lithiation) is an ideal material to optimize cycle stability and rate performance. Secondly, the nanosize and intrinsic characteristics of porous MoO_3 will provide both reversible large capacity and good electrical conductivity. Thirdly, the specific architectural feature of binder-free single-crystalline TiO_2 nanotube array will simplify the electrode fabrication process. Fourthly, TiO_2 nanotube array provides direct electron transport pathway between active material and current collector and also facilitate uniform deposition of porous MoO_3 with large areal mass loading. In contrast to the advantages, there are disadvantages as well, firstly, to get synergic capacity of both anatase TNAs and porous MoO_3 the potential window must be higher (0.005–3 V). Secondly, the solid electrolyte interface (SEI) layer is inevitable which leads to high capacity fading.

Experimental section

Synthesis of MoO_3/TNAs

Prior to anodic oxidation, titanium foil (0.125-mm-thick foil, 99.7 % purity, Sigma Aldrich) was degreased by

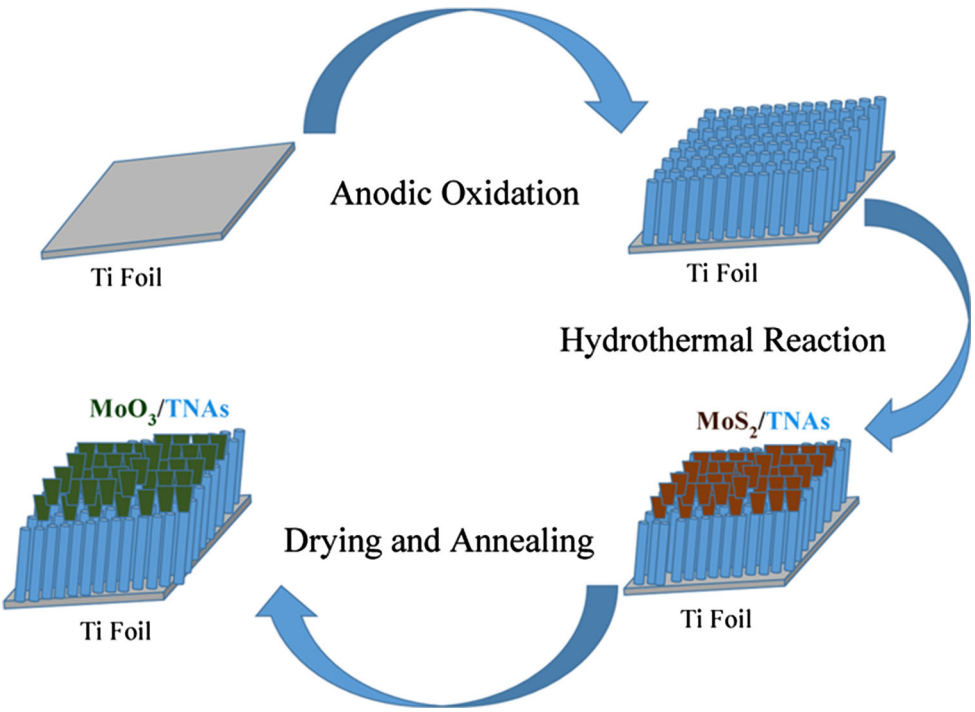

Fig. 1 Schematic illustration of the formation of MoO_3/TNAs composite: (I) Ti substrate; (II) formation of TNAs on Ti substrate; (III) grafting MoS_2 on TNAs via hydrothermal reaction (IV) formation of MoO_3/TNAs

sonication in acetone, ethanol and deionized water in turn, then dried in air. The electrochemical cell for anodization was a two-electrode cell, consisting of Ti foil as working electrode and platinum foil as counter electrode. Electrochemical anodization experiments were conducted at a constant potential with a DC power supply (DH1722A-2 110V/3A). The electrolyte was 0.3 wt% NH_4F and 2 vol.% water in ethylene glycol (99.8 %, anhydrous). All the tests were performed at room temperature. The TNAs were synthesized at the voltage of 50 V for 2 h. The as-prepared TNAs were annealed at 450 °C to transform its phase.

The porous MoO_3 were deposited by hydrothermal method reported elsewhere (Yu et al. 2014). The TNAs containing Ti substrate was placed against the wall of Teflon liner with interested surface downwards. The prepared 30 mL solution of $(NH_4)_6Mo_7O_{24}{\cdot}4H_2O$ (1 mmol) and thiourea (0.484 g) was transferred gently in Teflon-lined stainless steel autoclaves. Hereafter, the autoclave was sealed and maintained at 180 °C for different reaction time (2, 4, 6, 8, 10 h) and cooled down to room temperature spontaneously. The samples were collected and rinsed with distilled water for several times to remove the residual reactant and dried in vacuum oven at 80 °C for 30 min. Now MoS_2-deposited TNAs were obtained and annealed at 400 °C for 2 h to convert MoS_2 into MoO_3. For comparison, porous MoO_3 were grown in the similar way at titanium substrate.

Characterization

The surface and cross-sectional morphologies of the TNAs and MoO_3/TNAs were characterized using field emission scanning electron microscopy (FE-SEM LEO 1530). The phase structure of the TNAs, porous MoO_3 and MoO_3/TNAs were characterized by X-ray powder diffraction (XRD). The Cu $K\alpha$ radiation ($\lambda = 0.15$ nm) were used for XRD analysis. The electrochemical kinetics were studied by cyclic voltammetry (CV) test measured at a scan rate of 5 mV s^{-1} at a potential between 0 and 3 V.

Electrochemical characterization

The lithium storage performances of electrode were evaluated using Li| MoO_3/TNAs half-cells. The cells were 2032 coin cell and assembled in an argon-filled glove box. The cathode was MoO_3/TNAs without additives, the anode was lithium foil, and the separator is celgard 2300. The electrolyte is 1 M $LiPF_6$ dissolved in the mixture of ethylene carbonate (EC) and dimethyl carbonate (DMC) with volume ratio of 1:1. The cells were galvanostatically charged and discharged between 0.005 and 3 V (vs. Li/Li^+) at the current of 0.01 mA for the initial two cycles and then at 0.05 mA for the following cycles. The electrodes for comparison were configured and analyzed at same parameters.

Results and discussion

The synthesis process of porous MoO_3/TNAs is schematically illustrated in Fig. 1. Well oriented TNAs are synthesized at the nanostructured substrate via electrochemical anodization of Ti foil at room temperature (Fig. 1 I and II). MoS_2 is coated on the top of these vertical TNAs via hydrothermal reaction (Fig. 1 III) and oxygen annealing converts MoS_2 in MoO_3 (Fig. 1 IV).

The annealed TNAs and MoO_3/TNAs are characterized by SEM, as shown in supporting information Fig. S1 and S2, respectively. It is found that the TNAs were compact and uniform, without secondary nanostructures on the top or side surface (Fig. S1). The average inner diameter of the TNAs is around 60 nm and the length was about 3–5 μm. For MoO_3/TNAs sample, MoO_3 nanoflakes are grafted on the top of TNAs and the thickness of MoO_3 is controlled via deposition time (Fig. S2). The MoO_3 precipitate coat the surface partially when hydrothermal reaction was continued for 2 h (Fig. S2a) and the side of TNAs was almost as neat as pristine TNAs (inset Fig. S2b). As the hydrothermal duration increases to 4 h, both the top surface and side surface of TNAs are fully covered with MoO_3 nanoflakes and nanochannels were blocked (Fig. S2c, d). The MoO_3 nanoflakes with various lateral dimensions ranging in nanometers are grafted on the top, inner and outer surface of TNAs. The coating layer thickness increased linearly as reaction time increased as shown in Fig. S2. The TNAs might incorporate MoO_3 for stacking and control volumetric changes on lithiation. MoO_3 nanoflakes due to their 2D structure and high surface area can facilitate the transport of ions/electrons thus improve the response of system and recovery kinetics (Alsaif et al. 2014) (Fig. 2).

The α-MoO_3 is an anode material candidate for LIBs due to its stable layer structure which facilitates lithium insertion. The XRD pattern of MoO_3/TNAs indicates that diffraction peaks could be indexed to titanium (JCPDS NO. 44-1294), tetragonal anatase TiO_2 (JCPDS no. 21-1272) and orthorhombic α-MoO_3 (JCPDS no. 05-0508) (Fig. 2; Fig. S4). In detail, the peaks at 35°,38.4°,40.1°, 53°, 62.9°,70.6°, 74.1°, 76.2° and 77.4° represent Ti planes (100), (002), (101), (102), (110), (103), (200), (112) and (201), respectively. The peaks at 12.6°, 23.3°, 27.3° and 33.7°, can be attributed to α-MoO_3 (020), (110), (021), and (111) planes, respectively. The peaks at 25.0° and 47.9° can be attributed to (101) and (200) planes of anatase-TiO_2. The MoO_3 peak (040) at 25.7 overlaps with TiO_2 in composite. The anatase TiO_2 peaks could be observed in

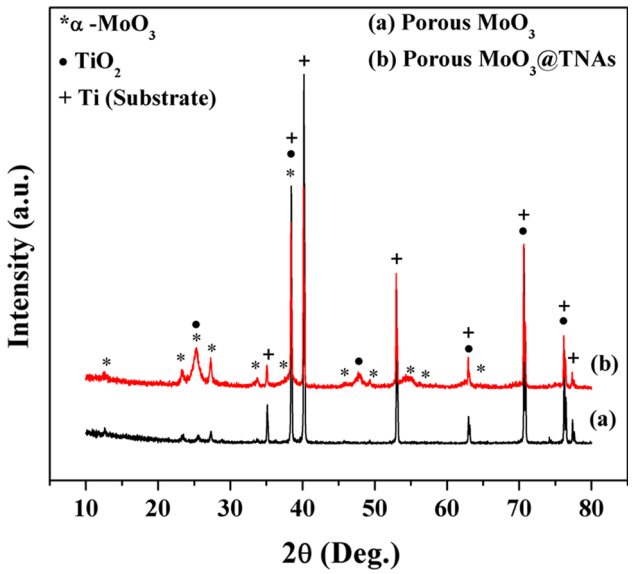

Fig. 2 XRD patterns of *(a)* porous MoO_3 *(b)* MoO_3/TNAs composite

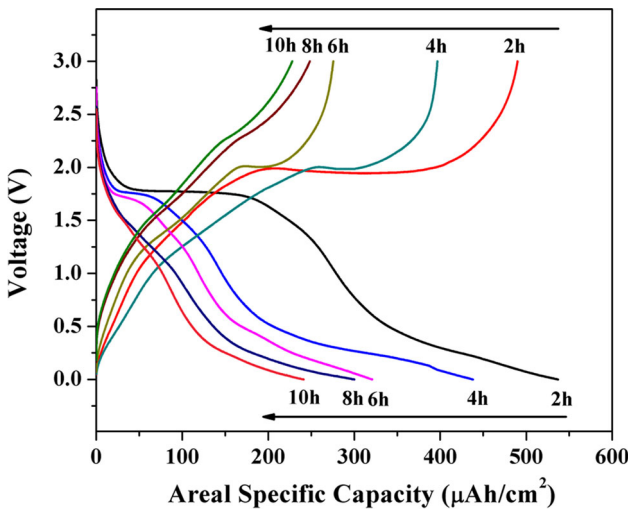

Fig. 3 The 3rd charge and discharge curves of MoO_3/TNAs synthesized for 2, 4, 6, 8 and 10 h at current density of 50 μA cm^{-2} at a potential of 0.005–3 V

only MoO_3/TNAs composite and porous MoO_3 did not show any anatase TiO_2 peak. The XRD of MoO_3/TNAs with standard data is shown in Fig. S4. These results suggest that adopted synthesis strategy successfully covers anatase TNAs with α-MoO_3 having good crystallinity without introducing other impurity phases.

The TNAs with fully covered surface may hinder Li^+ ion and electron recombination due to slow movement of electrons from oxide material which have low conductivity. As the thickness of coated oxide material increases, the movement of electron is hindered and reduces lithium intercalation. The electrochemical properties of MoO_3/TNAs synthesized for different times of 2–10 h were elucidated in Fig. 3. As the deposited layer of nanoflakes thickens with increasing reaction time so capacity decreases, consistent with literature (Guan et al. 2014a; Zhu et al. 2015). The Li insertion and extraction plateau can be observed till 6 h time duration which indicates incorporation of TNAs, but length of plateau decreases with increase in time. The plateau for 8 and 10 h fully disappeared indicating that incorporation of anatase TNAs diminished after long time duration which is attributed to thickness of MoO_3 which might hinder electronic and ionic recombination.

To optimize the highest capacity, the hydrothermal reaction is conducted for 3 h (Fig. 4a, b).The top surface of TNAs was partially covered with MoO_3 and upper orifices remain uncovered not to block nanochannels which facilitate Li ions transportation to the inner wall of nanotubes (Fig. 4a). The lateral sides of TNAs were grafted with MoO_3 (Fig. 4b). A suitable amount of MoO_3 deposition on top of TNAs is required for the best performance as anode material.

Anatase TiO_2 has a tetragonal structure (space group I41/amd), in which a Ti^{4+} ion is surrounded by a distorted oxygen octahedron while numerous vacant octahedral and tetrahedral sites exist between these octahedrons. Li ions are accommodated in these vacant sites. Two voltage plateaus appear near 1.7 and 1.9 V (vs. Li/Li^+) in the curves of the anatase TNAs and MoO_3/TNAs anodes, which demonstrate that TNAs are also contributing in MoO_3/TNAs while they are totally different from porous MoO_3. The one at 1.7 V (vs. Li/Li^+) in the negative scan corresponds to Li-ion insertion into TiO_2, while the other in the positive scan accords with Li-ion desertion. The total reaction for Li-ion insertion/extraction is described by (Guan et al. 2014a, b):

$$TiO_2 + xLi^+ + xe^- \leftrightarrow Li_xTiO_2 \quad (1)$$

Here, x could be up to 0.5, corresponding to a capacity of 168 mAh g^{-1}.

α-MoO_3 has an orthorhombic structure containing distorted MoO_6 octahedral. They share edges and form chains that are cross-linked through oxygen atoms to yield layers. The Li ions were accommodated in the interlayer space between these layers. Most of Li ions move easily, which is the cause of excellent reversibility. The total reaction for Li-ion insertion and extraction is described by (Guan et al. 2014a, b):

$$MoO_3 + xLi^+ + xe^- \leftrightarrow Li_xMoO_3 \quad (2)$$

It is known that the electrochemical properties not only depends on surface properties and crystallinity, but also depends upon the texture (Fan et al. 2013). The nanohybrid materials reduce Li ion diffusion path enabling electrolyte ions to be transported smoothly and pores

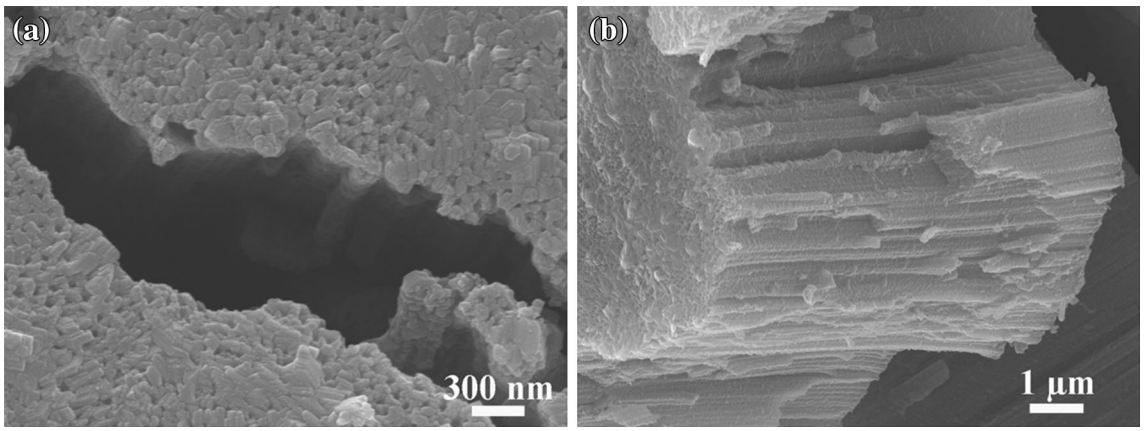

Fig. 4 MoO_3/TNAs for the time duration of 3 h: **a** top surface of TNAs, **b** lateral side of TNAs

provide large specific surface area which strongly suggests its potential applicability as an electrode material for LIBs (Moriguchi et al. 2006). The Li-ion intercalation behaviors of anatase TNAs, porous MoO_3 and MoO_3/TiO_2 are compared to study the effect of MoO_3 according to their electrochemical properties (Fig. 5).

The reaction kinetics is studied with the help of CV measured at a scan rate of 5 mV s^{-1} at 0–3 V, as shown in Fig. 5a–c. The cathodic peaks are observed at 0.6 and 1.45 V for the anatase TNAs, while 1.94 V for porous MoO_3 (Li et al. 2006; Ryu et al. 2012). The cathodic peaks for MoO_3/TNAs are observed at 0.66 V corresponding to the reduction of electrolyte solution and formation of solid electrolyte interface (SEI) layer on the surface of working electrode. The anodic peaks observed for anatase TNAs at 2.37 V, for porous MoO_3 at 1.52 V while for MoO_3/TNAs at 2.34 and 1.51 V were due to the delithiation from oxides (Li et al. 2006; Ryu et al. 2012).

The charge/discharge curves for the third cycle at current density of 50 µA cm^{-2} at potential window of 0.005–3 V are shown in Fig. 5d. The first two charge/discharge cycles are measured at the current density of 10 µA cm^{-2} to stabilize the charge and discharge. The third cycle discharge capacity is 287, 234 and 797 µAh cm^{-2} for anatase TNAs, porous MoO_3 and MoO_3/TNAs, respectively. The areal specific capacity for MoO_3/TNAs is three times higher than those of anatase TNAs and porous MoO_3. The electrochemical properties improve due to the combination of MoO_3 with high specific capacity and ordered TNAs with large surface area for efficient deposition and fast Li-ion kinetics. The anatase TiO_2 incorporating MoO_3 also helps to enhance capacity. A larger irreversible capacity is observed due to formation of SEI layer. The areal capacity increases when potential drops below 1.0 V. The slope below 0.7 V suggests Li ions intercalate into porous MoO_3 and MoO_3/TiO_2 according to following reaction (Guan et al. 2014a, b):

$$yLi_xMoO_3 + (6-x)yLi^+ + (6-x)ye^- \leftrightarrow yMo + 3yLi_2O \quad (3)$$

Li ions insert into anatase TNAs or react with electrolyte as potential drops below 0.5 V. The lithiation in MoO_3/TNAs appears in a different way. At lower voltage regions Li ions react with the solid solution (Li_xMoO_3) to form Mo metal and Li_2O oxides which are irreversible, but the nano-textured synthesis induces a reversible reaction of Li_2O during charging (Guan et al. 2014a, b).

Stable cyclic performance of electrode materials is important for practical application of lithium-ion batteries. Figure 6a depicts the cyclic performance and efficiency of anatase TNAs, porous MoO_3 and MoO_3/TNAs. The initial two cycles are charged/discharged at the current density of 10 µA cm^{-2} to stabilize the surface reactions and next charged/discharged cycles are at 50 µA cm^{-2}. The cyclic performance of anatase TNAs and porous MoO_3 are approximately similar and stable after few cycles. The composite electrode shows considerably enhanced charge/discharge capacity with respect to anatase TNAs and porous MoO_3 electrodes during all the 50 cycles. The MoO_3/TNAs nanostructure electrode exhibits a discharge capacity of 797 µAh cm^{-2} for third cycle and is stable after 25th cycle till 50th cycle (226 µAh cm^{-2}), which is much higher than those of the anatase TNAs, porous MoO_3 electrodes (84 and 129 µAh cm^{-2} for 50th cycles, respectively). The high capacity fading in initial cycles of MoO_3/TNAs might be attributed to the formation of SEI layer and conversion of Li_2O oxides. The efficiency of all samples is 100 % (Fig. 6a).

The rate performance of the three samples is measured with different current densities (50, 100, 150, 200, 250 and again 50 µA cm^{-2}). The rate capability of MoO_3/TNAs is the highest compared to anatase TNAs and porous MoO_3. After the current density switched back to 50 µA cm^{-2}, the capacity for MoO_3/TNAs is higher enough and more

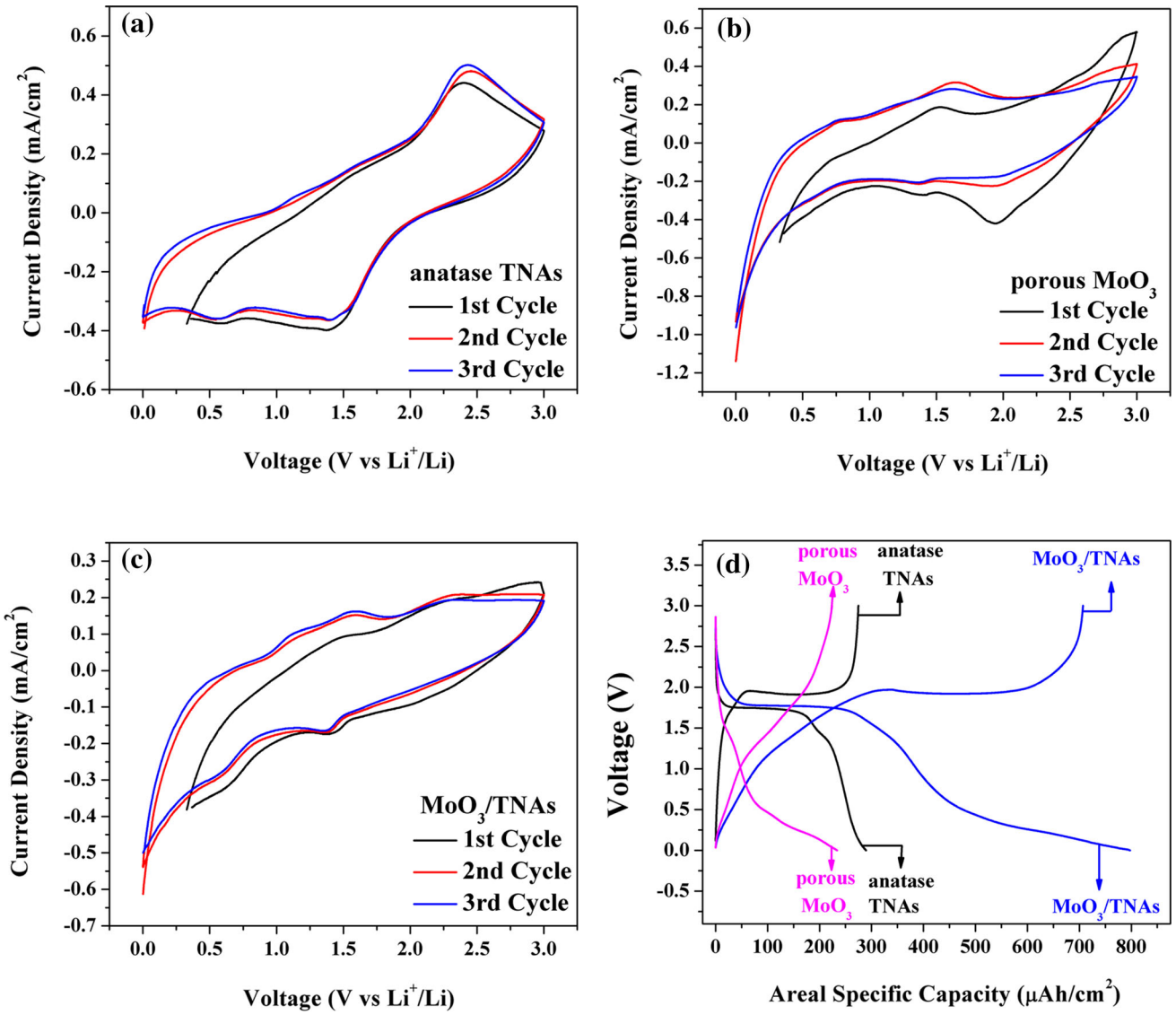

Fig. 5 Cyclic voltammetry curves of the anatase TNAs (**a**), porous MoO_3 (**b**) and MoO_3/TNAs (**c**), (**d**) the 3rd charge and discharge curve of anatase TNAs, porous MoO_3 and MoO_3/TNAs at current density of 50 μA cm^{-2} at a potential of 0.005–3 V

stable. These results reveal that the incorporation of anatase TiO_2 into MoO_3 nanostructures can greatly enhance the electrochemical performance for lithium storage.

The MoO_3/TNAs may be used as anode material in LIBs for achieving high capacity. However, thickness of grafted MoO_3 could be changed for achieving optimal results. Previously reported results and our present results are summarized in Table 1. Firstly, there are rare reports about MoO_3-grafted TNAs as anode material. The length of TNAs may play their role and specific capacity enhanced from 154.9 to 1340 μAh cm^{-2} for 1.6 and 9 μm, MoO_3-grafted TNAs, respectively. Although, specific capacity has been increased a lot, our results showed that MoO_3-grafted TNAs of small length (3 μm) exhibited higher specific capacity (797 μAh cm^{-2}) as compared to reported literature. It might be due to the fabrication process, synergetic effect of MoO_3-grafted TNAs and porous nature of MoO_3. The hydrothermal method is a wet method which may be helpful for covering all the voids of TNAs. Therefore, MoO_3 may fill TNAs which results in the present electrochemical properties. The lithium ion inserted in MoO_3 first and combination of MoO_3 with TNAs enhanced the lithium insertion/deinsertion, which results in higher capacity than anatase TNAs. The thickness of MoO_3 can be varied via fabrication method which brings exciting controllable performance of LIBs.

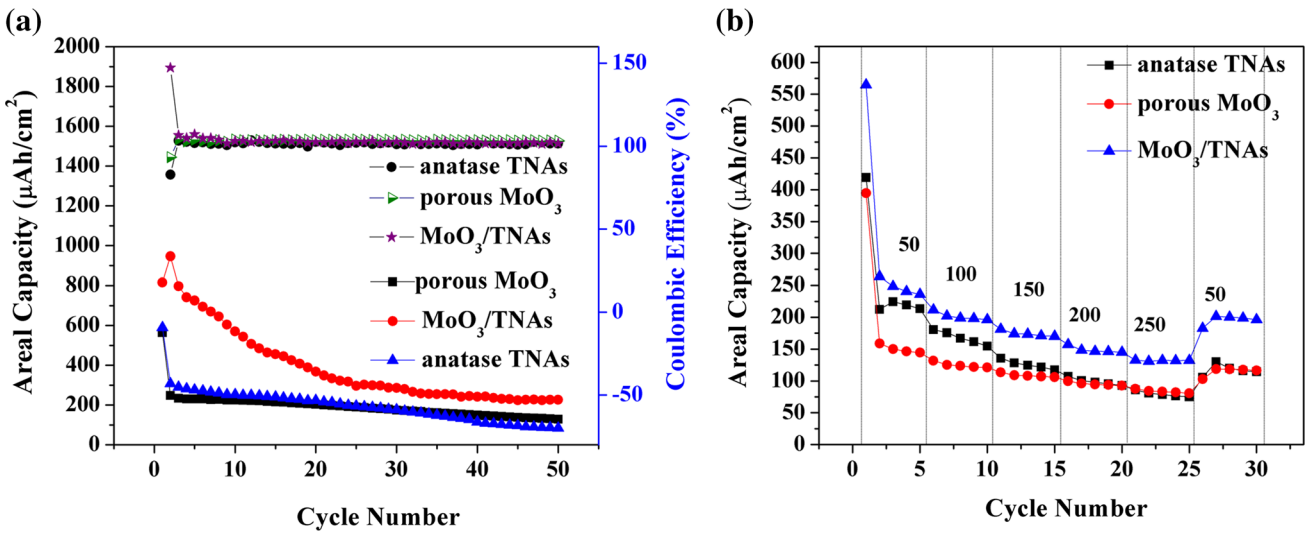

Fig. 6 **a** The cyclic performance and efficiency of anatase TNAs, porous MoO_3 and MoO_3/TNAs. **b** The rate performance of anatase TNAs, porous MoO_3, MoO_3/TNAs

Table 1 Comparison of Guan et al. MoO_3/TNAs and our synthesized MoO_3/TNAs

Material	MoO_3/TNAs (references)	MoO_3/TNAs (our work)
Coating method	Electrochemical	Hydrothermal
Titanium dioxide nanotube arrays length (μm)	1.6–9	3–5
1st discharge capacity (μAh cm^{-2})	1340 at 800 μA cm^{-2} (Guan et al. 2014a)	947 at 10 μA cm^{-2}
3rd discharge capacity (μAh cm^{-2})	154.9 at 50 μA cm^{-2} (Guan et al. 2014b)	797 at 50 μA cm^{-2}

Conclusion

TNAs were grown via anodic oxidation method and MoO_3 nanoflakes were grafted at TNAs via hydrothermal method for the first time. The optimal electrochemical properties of MoO_3/TNAs were obtained for 3 h deposition of MoO_3 nanoflakes. The specific capacity (~797 μAh cm^{-2}) of MoO_3/TNAs was three times higher than anatase TNAs (~287 μAh cm^{-2}) and porous MoO_3 (~234 μAh cm^{-2}). The rate performance and efficiency of LIB (in which MoO_3/TNAs used as anode material) were also enhanced. The anatase TiO_2 incorporates MoO_3 nanostructures and enhances the electrochemical performance, hence MoO_3/TNAs electrode might be a useful anode material for lithium ion micro-batteries. The carbon-free conducting nanocoated electrodes will be able to open new opportunities in the development of high-performance next-generation lithium-ion micro-batteries.

Acknowledgments This work is supported by the National Natural Science Foundation of China (Grant no. 21271114); Tsinghua University independent research and development fund (20111080982) and Program for Changjiang Scholars and Innovative Research Team in University (IRT13026).

References

Alsaif MMYA, Balendhran S, Field MR, Latham K, Wlodarski W, Ou JZ, Kalantar-zadeh K (2014) Two dimensional α-MoO3 nanoflakes obtained using solvent-assisted grinding and sonication method: application for H2 gas sensing. Sens Actuators B 192:196–204. doi:10.1016/j.snb.2013.10.107

Anwar T, Wang L, Tongxiang L, He X, Sagar RUR, Shehzad K (2015) Effect of aspect ratio of titanium dioxide nanotube arrays on the performance of lithium ion battery. Int J Electrochem Sci 10:6537–6547

Armstrong G, Armstrong AR, Bruce PG, Reale P, Scrosati B (2006) TiO_2(B) nanowires as an improved anode material for lithium-ion batteries containing LiFePO4 or LiNi0.5Mn1.5O4 cathodes

and a polymer electrolyte. Adv Mater 18:2597–2600. doi:10.1002/adma.200601232

Cao F-F, Wu X-L, Xin S, Guo Y-G, Wan L-J (2010) Facile synthesis of mesoporous TiO2 − C nanosphere as an improved anode material for superior high rate 1.5 V rechargeable Li ion batteries containing LiFePO4 − C cathode. J Phys Chem 114:10308–10313. doi:10.1021/jp103218u

Fan Y, Zhang N, Zhang L, Shao H, Wang J, Zhang J, Cao C (2013) Co3O4-coated TiO2 nanotube composites synthesized through photo-deposition strategy with enhanced performance for lithium-ion batteries. Electrochim Acta 94:285–293. doi:10.1016/j.electacta.2013.01.114

Fan J, Li G, Luo D, Fu C, Li Q, Zheng J, Li L (2015a) Hydrothermal-assisted synthesis of Li-rich layered oxide microspheres with high capacity and superior rate-capability as a cathode for lithium-ion batteries. Electrochim Acta 173:7–16. doi:10.1016/j.electacta.2015.05.028

Fan JM, Li GS, Luo D, Fu CC, Li Q, Zheng J, Li LP (2015b) Hydrothermal-assisted synthesis of Li-rich layered oxide microspheres with high capacity and superior rate-capability as a cathode for lithium-ion batteries. Electrochim Acta 173:7–16. doi:10.1016/j.electacta.2015.05.028

Gong J, Zeng W, Zhang H (2015) Hydrothermal synthesis of controlled morphologies of MoO3 nanobelts and hierarchical structures. Mater Lett 154:170–172. doi:10.1016/j.matlet.2015.04.092

Guan D, Wang Y (2013) Electrodeposition of Ag nanoparticles onto bamboo-type TiO_2 nanotube arrays to improve their lithium-ion intercalation performance. Ionics 19:879–885. doi:10.1007/s11581-012-0814-9

Guan D, Li J, Gao X, Yuan C (2014a) Controllable synthesis of MoO_3-deposited TiO_2 nanotubes with enhanced lithium-ion intercalation performance. J Power Sources 246:305–312. doi:10.1016/j.jpowsour.2013.07.096

Guan D, Li J, Gao X, Yuan C (2014b) Effects of amorphous and crystalline MoO_3 coatings on the Li-ion insertion behavior of a TiO_2 nanotube anode for lithium ion batteries. RSC Adv 4:4055–4062. doi:10.1039/C3RA44849E

Guo W, Xue X, Wang S, Lin C, Wang ZL (2012) An integrated power pack of dye-sensitized solar cell and Li battery based on double-sided TiO_2 nanotube arrays. Nano Lett 12:2520–2523. doi:10.1021/nl3007159

http://www.nature.com/srep/2013/130618/srep02007/abs/srep02007.html#supplementary-information

Kim HS, Kang SH, Chung YH, Sung Y-E (2010) Conformal Sn Coated TiO_2 nanotube arrays and its electrochemical performance for high rate lithium-ion batteries. Electrochem Solid State Lett 13:A15–A18. doi:10.1149/1.3264612

Kyerematen NA (2014) Self-organised TiO_2 nanotubes for 2D or 3D Li-ion microbatteries. ChemElectroChem 1:1442–1466. doi:10.1002/celc.201402109

Kyerematen NA, Lebouin C, Knauth P, Djenizian T (2013a) The electrochemical behaviour of TiO_2 nanotubes with Co_3O_4 or NiO submicron particles: composite anode materials for Li-ion micro batteries. Electrochim Acta 88:814–820. doi:10.1016/j.electacta.2012.09.120

Kyerematen NA, Vacandio F, Sougrati MT, Martinez H, Jumas JC, Knauth P, Djenizian T (2013b) Effect of Sn-doping on the electrochemical behaviour of TiO_2 nanotubes as potential negative electrode materials for 3D Li-ion micro batteries. J Power Sources 224:269–277. doi:10.1016/j.jpowsour.2012.09.104

Li W, Cheng F, Tao Z, Chen J (2006) Vapor-transportation preparation and reversible lithium intercalation/deintercalation of α-MoO3 microrods. J Phys Chem B 110:119–124. doi:10.1021/jp0553784

Liu D et al (2008) TiO_2 nanotube arrays annealed in N_2 for efficient lithium-ion intercalation. J Phys Chem C 112:11175–11180. doi:10.1021/jp801300j

Liu D et al (2009) TiO_2 nanotube arrays annealed in CO exhibiting high performance for lithium ion intercalation. Electrochim Acta 54:6816–6820. doi:10.1016/j.electacta.2009.06.090

Liu S et al (2012) Nanosheet-constructed porous TiO_2–B for advanced lithium ion batteries. Adv Mater 24:3201–3204. doi:10.1002/adma.201201036

Matiko JW, Grabham NJ, Beeby SP, Tudor MJ (2014) Review of the application of energy harvesting in buildings. Meas Sci Technol 25:012002

Meng X, Yao J, Liu F, He H, Zhou M, Xiao P, Zhang Y (2013) Preparation of SnO_2@C-doping TiO_2 nanotube arrays and its electrochemical and photoelectrochemical properties. J Alloys Compd 552:392–397. doi:10.1016/j.jallcom.2012.10.177

Moriguchi I, Hidaka R, Yamada H, Kudo T, Murakami H, Nakashima N (2006) A mesoporous nanocomposite of TiO_2 and carbon nanotubes as a high-rate Li-intercalation electrode material. Adv Mater 18:69–73. doi:10.1002/adma.200501366

Patil A, Patil V, Wook Shin D, Choi J-W, Paik D-S, Yoon S-J (2008) Issue and challenges facing rechargeable thin film lithium batteries. Mater Res Bull 43:1913–1942. doi:10.1016/j.materresbull.2007.08.031

Pikul JH, Gang Zhang H, Cho J, Braun PV, King WP (2013) High-power lithium ion microbatteries from interdigitated three-dimensional bicontinuous nanoporous electrodes. Nat Commun 4:1732. doi:10.1038/ncomms2747

Qiu Y, Yan K, Yang S, Jin L, Deng H, Li W (2010) Synthesis of size-tunable anatase TiO_2 nanospindles and their assembly into anatase@titanium oxynitride/titanium nitride–graphene nanocomposites for rechargeable lithium ion batteries with high cycling performance. ACS Nano 4:6515–6526. doi:10.1021/nn101603g

Reddy MV, Subba Rao GV, Chowdari BVR (2013) Metal oxides and oxysalts as anode materials for Li ion batteries. Chem Rev 113:5364–5457. doi:10.1021/cr3001884

Ren Y, Liu Z, Pourpoint F, Armstrong AR, Grey CP, Bruce PG (2012) Nanoparticulate TiO_2(B): an anode for lithium-ion batteries. Angew Chem Int Ed 51:2164–2167. doi:10.1002/anie.201108300

Ryu W-H, Nam D-H, Ko Y-S, Kim R-H, Kwon H-S (2012) Electrochemical performance of a smooth and highly ordered TiO_2 nanotube electrode for Li-ion batteries. Electrochim Acta 61:19–24. doi:10.1016/j.electacta.2011.11.042

Wang J, Zhou Y, Hu Y, O'Hayre R, Shao Z (2011) Facile synthesis of nanocrystalline TiO_2 mesoporous microspheres for lithium-ion batteries. J Phys Chem C 115:2529–2536. doi:10.1021/jp1087509

Wang X, Xiang Q, Liu B, Wang L, Luo T, Chen D, Shen G (2013) TiO_2 modified FeS nanostructures with enhanced electrochemical performance for lithium-ion batteries. Sci Rep. doi:10.1038/srep02007

Wu J, Hong H (2014) Investigation of metal oxide/carbon nanotubes as anode material for high capacity lithium-ion cells. Meeting Abstracts MA2014-02:370

Wu HB, Chen JS, Hng HH, Wen Lou X (2012a) Nanostructured metal oxide-based materials as advanced anodes for lithium-ion batteries. Nanoscale 4:2526–2542. doi:10.1039/C2NR11966H

Wu QL, Li J, Deshpande RD, Subramanian N, Rankin SE, Yang F, Cheng Y-T (2012b) Aligned TiO_2 nanotube arrays as durable lithium-ion battery negative electrodes. J Phys Chem C 116:18669–18677. doi:10.1021/jp3072266

Xiong P, Liu B, Teran V, Zhao Y, Peng L, Wang X, Yu G (2014) Chemically integrated two-dimensional hybrid zinc

manganate/graphene nanosheets with enhanced lithium storage capability. ACS Nano 8:8610–8616. doi:10.1021/nn5041203

Xue L, Wei Z, Li R, Liu J, Huang T, Yu A (2011) Design and synthesis of Cu6Sn5-coated TiO_2 nanotube arrays as anode material for lithium ion batteries. J Mater Chem 21:3216–3220. doi:10.1039/C0JM03819A

Yang M, Yang G, Spiecker E, Lee K, Schmuki P (2013) Ordered "superlattice" TiO_2/Nb_2O_5 nanotube arrays with improved ion insertion stability. Chem Commun 49:460–462. doi:10.1039/C2CC37226F

Yu L, Wang Z, Zhang L, Wu HB, Lou XW (2013) TiO_2 nanotube arrays grafted with Fe_2O_3 hollow nanorods as integrated electrodes for lithium-ion batteries. J Mater Chem A 1:122–127. doi:10.1039/C2TA00223J

Yu X, Wang L, Liu J, Sun X (2014) Porous MoO_3 film as a high-performance anode material for lithium-ion batteries. ChemElectroChem 1:1476–1479. doi:10.1002/celc.201402145

Zhang Y, Yang Y, Xiao P, Zhang X, Lu L, Li L (2009) Preparation of Ni nanoparticle–TiO_2 nanotube composite by pulse electrodeposition. Mater Lett 63:2429–2431. doi:10.1016/j.matlet.2009.08.019

Zhao G, Zhang N, Sun K (2013) Electrochemical preparation of porous MoO_3 film with a high rate performance as anode for lithium ion batteries. J Phys Chem A 1:221–224. doi:10.1039/C2TA00361A

Zhu Q, Hu H, Li G, Zhu C, Yu Y (2015) TiO_2 nanotube arrays grafted with MnO_2 nanosheets as high-performance anode for lithium ion battery. Electrochim Acta 156:252–260. doi:10.1016/j.electacta.2015.01.023